Fast and High-Resolution NLoS Beam Switching over Commercial Off-the-Shelf mmWave Devices

Xueyang Hu, Tian Liu, and Tao Shu

Abstract—The high directionality of mmWave communication makes its line-of-sight (LoS) path susceptible to blockage when the user is moving. Most existing solutions have very stringent requirements on the antennas of the transmitter and the receiver, which are hardly met by today's consumer-level commercial off-the-shelf (COTS) mmWave products. In reality, a COTS device uses low-resolution wide-beam antennas, and hence cannot support the aforementioned methods for NLoS beam switching in response to the LoS blockage. In this paper, we develop a new method to support high-resolution mmWave multi-path channel resolving based on coarse-grained wide-beam phased array antennas. We design a novel real-time beam-switching algorithm that allows COTS devices to estimate the location and reflection coefficient of the dominant reflectors. Whenever the current LoS is blocked, our algorithm can compute in real-time the best alternative beam direction based on estimated reflectors to establish a strong NLoS link. We implemented the proposed algorithm on a COTS mmWave device and evaluated the system's performance on the physical and transport layer. Our experiments demonstrate the effectiveness of our algorithm on estimating dominant reflectors and calculating strong alternative beam directions, and its efficacy in providing robust connections for COTS mmWave devices.

Index Terms—mmWave communication, commercial off-the-shelf devices, non-line-of-sight, beam-switching.

1 Introduction

Millimeter-wave (mmWave) communication is considered as one of the most promising technologies for the next generation high-speed wireless networks [1], [2], [3]. In contrast to current WiFi and LTE-based 4G communications that operate at sub-6 GHz frequencies, mmWave network works at a much higher frequency band, therefore is able to provide much wider bandwidth for wireless applications [4], [5], [6]. For example, a mmWave link working at 60 GHz can support a data rate more than 7 Gbps [7]. Such a high-throughput transmission fits well with data-hungry real-time applications such as live high-definition video streaming and virtual reality (VR), which are envisioned to be the dominant killer applications in the era of 5G [8], [9].

Although mmWave provides many desirable features, a big challenge for its practical application is the susceptibility to line-of-sight (LoS) blockage [10], [11], [12]. In particular, the mmWave transmission relies on directional communication to overcome the high oxygen attenuation and the signal's propagation heavily relies on LoS [13], [14]. When the LoS is blocked by an obstacle, the mmWave signal can not penetrate through or circumvent around the obstacle, leading to a significant drop of the received signal strength. In this situation, one solution is to promptly steer the communication beam towards a strong non line-of-sight (NLoS) signal propagation path to maintain the communication [15].

Many methods have been proposed to find such a strong NLoS path in the literature, which can be divided into three categories. The first category uses beam-scanning to search over the space when a strong NLoS path is needed [16], [17], [18], [19]. The proposed methods include sequential scanning through the space and hierarchical scanning, which begins with a low-resolution scanning over the entire space, followed by iterative higher-resolution scannings over particular smaller (finer) ranges of directions that are selected based on the outcome of the previous round lower-resolution scanning. The average overhead of the scanning is usually around 100 ms to 200 ms [20], [21]. The second category assumes a nominal mmWave multi-path channel model, and then attempts to estimate the parameters of this model, including the amplitude, angle of departure (AoD), angle of arrival (AoA), and phase shift of each signal propagation path, by reverse engineering. For example, in [22], [23], based on a measured channel impulse response (CIR), reverse engineering is performed to find the optimal channel parameters that best match the nominal multi-path channel model with the measured CIR. The third category includes those well-studied array signal processing techniques, such as MUSIC [24] and ESPRIT [25], [26], that are pertinent to phased array antennas. These techniques conduct angular spectrum analysis over signals received at each antenna element to resolve the multi-path channel.

Despite their good performance, these existing methods all have very stringent/high requirements on the antennas of the transmitter and the receiver, which are hardly met by today's consumer-level commercial off-the-shelf (COTS) mmWave products. More specifically, since the methods in Category 1 require sequential scanning through N different beam patterns, each of which covers a non-overlapping $(360/N)^\circ$ slice of the space, the fundamental limitation of the methods is that the spatial resolution of the beam scanning is upper bounded by the minimum beam width of the phased-array antenna. When these methods are directly

The authors are affiliated with the Computer Science and Software Engineering Department of Auburn University at Auburn, AL 36849, USA. Emails: {xzh0051, tzl0031, tshu}@auburn.edu

applied to the coarse-grained wide-beam antenna, they may fail to identify those paths that happen to fall within the same beam pattern. As a result, signal propagation paths whose AoDs (or AoAs) are separated less than the minimum beam-width of the antenna would not be distinguishable. Therefore, to be able to accurately locate a strong NLoS path, these methods require the use of a narrow-beam horn antenna or a high-precision narrow-beam phased array antenna that has a large number of antenna elements, typically costs over $10K. Clearly such a high price tag is unaffordable to a COTS device. As a matter of fact, current COTS mmWave products typically use a quasi-omni-directional antenna (e.g., 180° beam width) for reception, and a coarse-grained wide-beam (e.g., 60° beam width) phased-array antenna for transmission [27], [28]. Similar issue exists in the methods of Category 2. In particular, to measure the CIR, the receive antenna needs to be able to accurately separate, measure, and report both the amplitude and the phase of each lag of the CIR components (in a typical indoor environment where a COTS mmWave device operates, the length of a lag is in the order of nanoseconds). Such a high-time-resolution CIR time-sequence information is typically not provided by COTS devices. Similarly, the array-signal angular spectrum analysis techniques in Category 3 require the accurate amplitude and phase information of the signal received at each individual antenna element. While a COTS receiver indeed reports the amplitude information of the aggregate signal combined from all antenna elements, it typically does not provide detailed amplitude and phase information of the received signals at individual antenna elements.

Due to the above limitations, the aforementioned methods are not directly applicable to consumer-level COTS mmWave devices. Only recently, several new path resolving methods that are suitable for COTS devices are proposed. Among them, non-coherent compressive path tracking proves to be the most effective algorithm, e.g., see [29], [30], [31], [32], [33]. Based on reverse engineering, this algorithm aims to find the direction of the strongest NLoS path by using only the signal's amplitude information. Instead of relying on a measured CIR, the algorithm probes the channel by sending out a sequence of compressive beacons, each of which is separated apart in time by a dozen microseconds. By measuring the amplitude of each received beacon on the receiver side, the algorithm finds the optimal AoA and AoD that best match the sequence of amplitudes calculated according to the nominal channel model to that of the received beacons. While upon each channel probing (i.e., the transmission of a group of compressive beacons) this method is able to obtain the strongest NLoS path of that moment, it incurs high channel-probing overhead when one needs to keep tracing the change of the strongest NLoS path. For instance, this happens for a user playing an electronic VR game, whereby the direction of the strongest NLoS path keeps changing due to the user's movement. Due to this reason, compressive sensing-based approach is mostly suitable for dynamic application scenarios with frequently changing environment and moving users, under which repetitively probing the channel to catch up with the frequent movement of reflectors in the environment is necessary. However, for those application scenarios where the environment is mostly static but the user could be moving, which are typical in most of the household applications, such repetitive probing may not be an efficient solution, as the reflectors in the environment are hardly changed.

Keeping the limitations and weaknesses of existing methods in mind, in this paper we are interested in developing a new method to achieve high-resolution mmWave multi-path channel resolving result using coarse-grained wide-beam phased array antennas that are commonly equipped on today's COTS mmWave devices. Based on this new method, we further propose an efficient computation-based beam-switching algorithm that can directly predict a strong NLoS path (i.e., without the overhead of per-prediction probing) whenever the LoS blockage happens and a strong NLoS backup path is needed. With these efforts, it becomes feasible for a commercial available device to perform fast and high-resolution NLoS beam switching. Our proposed method is most suitable for static-environment application scenarios, thus fills into the regime where the non-coherent compressive path tracking method does not perform efficiently.

More specifically, to address the challenge of achieving high-resolution multi-path channel resolving based on a coarse-grained wide-beam antenna array, we perform fine-grained spatial scanning of the antenna array and exploit the high spatial resolution of the differential received signal strength (RSS) information measured when the antenna array is turned to point to different directions with small steps. One key insight here is that the wide beam-width of the antenna array does not prevent the array from turning to scan the space in a fine resolution (e.g., with a step of 1° increment in the direction of the antenna beam). The differential RSS information associated with the spatial scanning process, which naturally has a high spatial resolution (e.g., in a resolution of 1°), is then exploited by a novel two-step multi-path channel resolving algorithm. In particular, a low-resolution out-lobe resolving step is first performed to identify the clusters of paths that are separated more than the beam width of the antenna array. Then, for each cluster, a high-resolution in-lobe resolving step is performed, which utilizes reverse engineering to compute the optimal in-cluster fine-grained paths that offer the closest match with the measured RSS of that cluster.

Our reflector-based NLoS beam-switching mechanism is then built upon the above channel resolving process. In particular, our method consists of two phases: the offline site survey phase and the online operational phase. In the site survey phase, our model aims to construct a reflector map by estimating the locations and reflection coefficients of the dominant reflectors in the environment, through a sequence of coordinated differential RSS measurements at multiple locations. At each location, the above channel resolving process is called to compute the top-K strongest NLoS paths generated by the dominant reflectors. Exploiting the sparse nature of the mmWave channel, the NLoS paths computed at different locations are then used to estimate the location of the dominant reflectors. Furthermore, based on the Fresnel reflection model assumption, the reflection coefficient of each dominant reflector is calculated by a minimum mean square error (MMSE) estimator based on the RSS measurements. Note that the offline site survey phase is basically a

one-time operation for static or quasi-static environments. The next offline site survey is not needed until there is a significant change on the layout of the environment (e.g., a new steel furniture is just added so the reflection layout is changed).

This reflector map is subsequently used in the online operational phase to calculate the supposedly strongest NLoS path at the current location of the user. Note that during this phase, our system can instantly calculate the NLoS path and does not require any additional probing effort. The main beam of the transmit antenna is then steered accordingly to maintain the ongoing connection when the LoS is blocked.

To verify the performance of the proposed method, we implement our algorithm on a COTS mmWave device MikroTik WAP 60G transceiver set [28].The system is tested in an indoor environment for both static and mobile applications. The results show that our system is able to accurately estimate the locations of the strong reflectors in the test environment. In case of LoS blockage, by steering the transmit antenna towards the directions indicated by the proposed algorithm, the system is able to achieve a 200% to 300% throughput gain over the case that the transmit antenna is always pointing to the LoS direction. Our received signal strength indicator (RSSI) measurement at the physical layer also shows that our algorithm can recover the link performance more quickly from blockage and achieves better stability than the device's built-in 802.11ad based method.

The remainder of the paper is organized as follows. We present our system design in Section 2. The test-bed implementation is described in Section 3. The test settings and test results are presented in Section 4. And we conclude our paper in Section 5.

2 System Design

2.1 Problem Statement and Solution Framework

We consider an indoor mmWave communication scenario where the room layout is static, and there is only one link consisting of one mmWave access point (AP) and one mmWave adapter (referred to as the client). Without loss of generality, we consider an uplink case: the AP is the receiver and the client is the transmitter. Just like those consumer-level off-the-shelf mmWave products, we assume the AP uses a quasi-omni-directional beam pattern for receiving, while the client is equipped with a low-end phased array antenna with coarse beamforming capability for directional transmission.

For indoor mmWave communication, a strong NLoS path is used to maintain the connection when LoS is being blocked. In a static communication scenario where both the transmitter and the receiver are located at fixed positions, the NLoS paths should also remain static therefore can be measured in advance. However, what we consider here is a more common but challenging scenario: the AP is static but the client is mobile, e.g., in a wireless VR game, making the NLoS paths change as the client moves . The pre-measurement method will fail under this scenario due to the infinite number of possible transmitter locations. So how to determine the real-time NLoS paths for a mobile transmitter is the problem we are trying to solve here.

Fortunately, the strong NLoS paths are not randomly distributed. Instead, they are heavily dependent on the locations of the transmitter, the receiver, and the mmWave signal reflectors in the environment. Specifically, the high frequency of mmWave and the usage of transmit antenna array make the communication quasi-optical: in a typical indoor environment such as an office or home, most of the strong NLoS paths are formed by the first-order specular reflection from reflectors in the environment. Note that we are mainly focused on indoor applications in a small-to-moderate-size room, where the likelihood for the existence of some reflective surfaces, such as concrete walls and book shelves, is high. Due to the wide availability of these reflective objects, the NLoS paths generated by these reflectors can cover most area of the room. Therefore the assumption that there exists a strong NLoS path should be reasonable for the indoor scenarios considered in this work.

Based on this fact, we take a generative method to solve our real-time NLoS paths resolution problem. In particular, we intend to create a model for dominant reflectors in the environment based on some site survey process. This model describes the location, orientation, and reflection coefficient of each dominant reflector. We then put the model into operation: at a given client location, the real-time NLoS paths are simply computed as the specular reflections generated by those dominant reflectors according to the model.

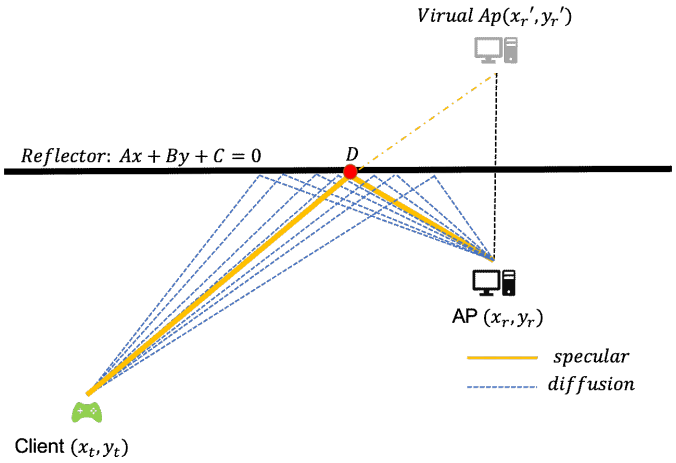

Fig. 1: First order reflection model.

This idea is better illustrated in Figure 1, where the locations of the client and the AP are (x_t, y_t) and (x_r, y_r), respectively. And we assume there is only one reflector R (the solid black line) for simplicity of presentation. Clearly, given (x_t, y_t), (x_r, y_r), and the location and orientation of the reflector R, there is a unique path, highlighted in yellow in Figure 1, by which the signal transmitted from the client can be specularly reflected by the reflector, and received by the AP. The uniqueness of this path is owing to the law of reflection, i.e., in the case of specular reflection, for each incident ray, the angle of incidence equals the angle of reflection. It is easy to verify that point D is the only position on the reflector through which the incident ray from the client can be specularly reflected and received by the AP, while other positions on the reflector contribute to the weak diffusive scattering, as denoted by the blue dotted

lines. Here, point D is the intersection between reflector R and the line segment connecting the client and the mirrored image of the AP (referred to as virtual AP), defined w.r.t. the reflector. Consequently, the reflection-induced NLoS path cluster simply consists of a strong specular reflection path (the solid yellow path), surrounded by a set of weak diffusive reflection paths (the dotted blue paths).

The insight is that point D can be uniquely decided by the AoD (say α) and the AoA (say β) of the specular reflection path: it is just the intersection between a line passing through the client with an orientation of α and a line passing through the AP with an orientation β. Therefore, given α and β are known, the location and orientation of the reflector R can be uniquely decided by two independent sets of AP and client locations. However, β is unknown in our problem setting, due to the omni-directional receive antenna of the AP. This condition poses challenges to the reflector modeling.

We propose the following approach to address the above challenge in the localization of R. The reflector in a 2-D space can be modeled as a line segment with math representation $Ax + By + C = 0$ ($A, B, C \in \mathbf{R}$), where $\mathbf{R}$ is the set of real numbers. In this assumption, we do not consider the actual length of the reflector, because in reality the size of a dominant reflector is usually big enough to cover most of the locations through reflection in a small-to-moderate-size room, which is the setting of interest considered in this work. Let the AP's position be (x_r, y_r), and the client's location be (x_t, y_t). Denote the location of the virtual AP by (x'_r, y'_r). The location of the virtual AP satisfies the following condition:

$$\begin{cases} A\dfrac{x_r + x'_r}{2} + B\dfrac{y_r + y'_r}{2} + C = 0 \\ \dfrac{A(y'_r - y_r)}{B(x'_r - x_r)} = 1. \end{cases} \tag{1}$$

The virtual AP's location can be further calculated as:

$$\begin{cases} x'_r = \dfrac{(B^2 - A^2)x_r - 2ABy_r - 2AC}{(A^2 + B^2)} \\ y'_r = \dfrac{(A^2 - B^2)x_r - 2ABx_r - 2BC}{(A^2 + B^2)}. \end{cases} \tag{2}$$

Next we will find another constraint for the virtual AP's location. Let ϕ be the angle of departure (AoD) of the specular ray ($\phi \neq \frac{\pi}{2}$). Then the incidence part of the specular reflection path can be represented by:

$$tan(\phi)(x - x_t) = (y - y_t). \tag{3}$$

The incidence ray follows the law of reflection: the incident angle equals to the reflection angle. So the location of the virtual AP must satisfy Eq.(3). Substituting (x'_r, y'_r) into the equation, we get:

$$y'_r = tan(\phi)(x'_r - x_t) + y_t. \tag{4}$$

Substituting Eq.(4) into Eq.(2), we have:

$$\begin{aligned} &tan(\phi)(\frac{(B^2 - A^2)x_r - 2ABy_r - 2AC}{(A^2 + B^2)} - x_t) \\ &= (\frac{(A^2 - B^2)x_r - 2ABx_r - 2BC}{(A^2 + B^2)} - y_t). \end{aligned} \tag{5}$$

Eq.(5) provides an analytical condition that must be met by the locations of the AP and the client, the AoD, and the location and orientation of the reflector. Because the locations of the AP and the client can be measured, and (x_r, y_r) and (x_t, y_t) are considered known. Meanwhile, as will be clarified in Section 2.2, the AoD ϕ of the specular reflection path can be estimated through a sequence of RSS measurements accompanying the steering of the wide-beam transmit antenna. So ϕ is also considered as a known value. Therefore, Eq.(5) only depends on variables A, B, and C. As a result, we need at least three independent sets of $< \phi, (x_t, y_t) >$ to uniquely determine the location and orientation of the reflector.

To the best of our knowledge, this is the first framework in the literature that supports the computation of the reflector's location and orientation without knowing AoA, neither any phase information of the received signal. Our framework does require some knowledge on AoD, but the acquisition of this information does not rely on high-precision narrow-beam transmit antennas or any phase information of the signal, as will be described in Section 2.2. This is in sharp contrast to existing methods that rely on high precision phased array antennas and the phase information on both sides of the link to obtain accurate AoA and AoD in order to localize the reflectors [26].

2.2 Locating Dominant Reflectors

2.2.1 Design Philosophy

Dominant reflectors are reflectors that create strong NLoS paths for most of the indoor positions. Although the number of reflectors a mmWave radio can see vary with the device's location, there are only a few dominant reflectors in a realistic environment because of the sparsity of the mmWave channel, and most of dominant reflectors are static metallic surfaces that have low reflection losses.

We already show that a reflector can be uniquely determined by three independent sets of $< \phi, (x_t, y_t) >$, so deriving the AoD of the specular ray associated with the dominant reflectors (i.e., ϕ_i, for the i-th dominant reflector) is a crucial step in determining the dominant reflectors' location and orientation. We propose to determine ϕ_i's by measuring the RSS at the receiver as a function of the beam direction of the transmit antenna. In particular, let θ_{mid} denote the center angle of the main lobe of the transmit antenna. Given an omni-directional receive antenna, the RSS at the receiver is a function of θ_{mid}, denote as $P_r(\theta_{mid})$ and is given by

$$P_r(\theta_{mid}) = P_t \left\| \sum_{i=0}^{N} D(\theta_{mid}|\phi_i) g_i e^{j\delta_i} \right\|^2, \tag{6}$$

where P_t is the transmit power, and we have assumed that the mmWave channel has $N + 1$ paths (so there are N dominant reflectors), and the i-th path has a path loss, AoD, and path phase shift of g_i, ϕ_i, and δ_i, respectively. e is the natural logarithm, and j is the imaginary unit. $D(\phi_i|\theta_{mid})$ is the transmit antenna gain at the AoD ϕ_i, given that the main beam of the antenna is pointing at θ_{mid}. Without loss of generality, we assume $D(\phi_i|\theta_{mid}) = 1$ if $|\phi_i - \theta_{mid}| \leq \Theta_{beam}$ and $D(\phi_i|\theta_{mid}) = 0$ otherwise, where $2\Theta_{beam}$ is the beam width of the main lobe of the transmit antenna.

Clearly, according to Eq.(6), ϕ_i's can be easily resolved by steering a narrow-beam transmit antenna with small Θ_{beam} to perform a 360°-scanning of the space. However, note that in our problem we have a low-end phased array antenna with a wide beam-width. The reduced angle resolution (i.e., large Θ_{beam}) makes it challenging to resolve the ϕ_i's.

One way to resolve ϕ_i's is through reverse engineering, i.e., by considering (ϕ_i, g_i, δ_i)'s as variables, and then resolve them by solving a set of nonlinear equations defined by Eq.(6), where P_r is measured at multiple θ_{mid}'s. In this case, the optimal N^o and $(\phi_i^o, g_i^o, \delta_i^o)$, $0 \leq i \leq N^o$, can be simply calculated as the optimal solution to the following minimum mean square error (MMSE) problem:

$$\text{minimize} \frac{1}{2\pi} \int_0^{2\pi} |P_r(\theta_{mid}) - P_r^{\text{m}}(\theta_{mid})|^2 d\theta_{mid}, \quad (7)$$

where $P_r(\theta_{mid})$ is defined in Eq.(6) and $P_r^{\text{m}}(\theta_{mid})$ is the RSS measurements.

Although the above method fits in our problem and provides promising solutions, the computation complexity is high, which makes it unsuitable for COTS devices. In addition, it provides more than what the problem needs. Notice that, for the purpose of finding a NLoS backup path, what we are interested in is only the top few (say K, where K is a small integer) dominant reflectors that provide the strongest NLoS paths. Therefore, resolving the whole set of NLoS paths, as in the MMSE method, is unnecessary. Based on this observation, we propose to only consider the K particular θ_{mid}'s that correspond to the top-K RSS peaks in the function $P_r^{\text{m}}(\theta_{mid})$, and use these K θ_{mid}'s to estimate the AoDs of the top-K dominant reflectors in the environment.

This idea can be better illustrated as follows. We begin with the simplest scenario: suppose we only have one reflector, say R_1, in the environment. The specular reflection direction to R_1 is denoted as ϕ_1, as shown in Figure 2a. As the transmit antenna scans from $\theta_{mid} = 0$ to 360°, the RSS measured at the AP should present a trapezoid shape as shown in Figure 2b, where the high RSS level in the range of $\phi_1 - \Theta_{beam} \leq \theta_{mid} \leq \phi_1 + \Theta_{beam}$ is due to the fact that the AoD of the specular ray ϕ_1 is within the main lobe when the transmit antenna is scanning in this range. So, for the single-reflector case, the peak of the RSS, defined as the center of the RSS high level, corresponds to the AoD of the specular ray ϕ_1, as shown in Figure 2b.

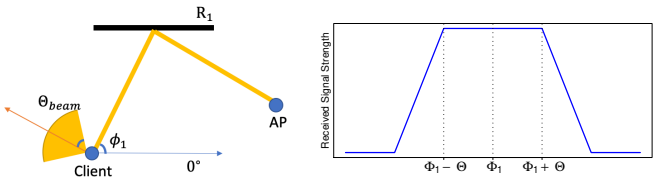

(a) Single reflector specular reflection case. (b) RSS pattern of single reflector.

Fig. 2: Single reflector scenario.

Now let us consider a more complicated scenario where there are two reflectors in the environment, as shown in Figure 3a, where AoDs of the two specular rays are denoted by ϕ_1 and ϕ_2, respectively. Without loss of generality, we assume that $\phi_1 < \phi_2$. Note that if ϕ_1 and ϕ_2 are separated far apart such that $\phi_2 - \phi_1 > 2\Theta_{beam}$, then each of the two AoDs can be resolved separately as two independent single-reflector cases (i.e., the two peaks of the RSS curve correspond to ϕ_1 and ϕ_2 respectively). Now let us consider the case that ϕ_1 and ϕ_2 are close enough such that $\phi_2 - \phi_1 \leq 2\Theta_{beam}$. In this case, as the transmit antenna scans from $\theta_{mid} = 0$ to 360°, the RSS measured at the AP should present the pattern shown in Figure 3b, where the different levels of RSS are due to the fact that different combinations of the specular rays are in the main lobe as the transmit antenna scans. Clearly, in this case, the peak of the measured RSS corresponds to the center angle of ϕ_1 and ϕ_2, i.e., $\frac{1}{2}(\phi_1 + \phi_2)$. Physically, this means that because ϕ_1 and ϕ_2 are close to each other, the reflectors R_1 and R_2 are actually considered as a cluster of reflectors, and the peak of the measured RSS simply corresponds to the center AoD of this cluster.

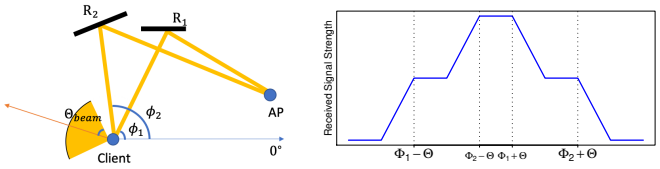

(a) Multiple reflectors specular reflection case. (b) RSS pattern of multiple reflectors.

Fig. 3: Multiple reflectors scenario.

To simplify the presentation, we have assumed that the beam pattern of COTS devices has a regular pie shape, but the insight here is general enough to accommodate any regular/irregular beam pattern function. This is because changing the beam pattern only changes the coefficients of antenna gain, but does not change the structure/nature of the problem.

Note while Figures 2b and 3b are showing symmetric RSS peaks in concept, the measured RSS peaks in reality are rarely symmetric. As shown in Figure 4, the measured peaks are usually skewed, mainly due to the large number of scatters (i.e., small/minor reflectors) surrounding the major reflector and the heterogeneous reflection efficiency of the reflectors. Therefore, while a measured RSS peak provides a rough range of directions where one or several major reflectors could reside in, simply interpreting the mid-point of the RSS peak as the AoD of one major reflector is inaccurate and misleading, for the peak could be generated by multiple close-by major reflectors.

How to accurately resolve the major reflector(s) from the skewed RSS measurements constitutes a challenge.

2.2.2 *Two-step Fine-Grained Multi-path Channel Resolving*

We solve this challenge by a novel two-step multi-path channel resolving algorithm. The main idea is to first identify clusters of major reflectors by evaluating the peaks of measured RSSI, and then apply reverse engineering within each RSSI peak to resolve the optimal in-cluster reflector setting that offers the best match with the measured RSSI in that peak.

The detail of our algorithm is described below:

(1) Low-resolution out-lobe resolving: Since the goal of the algorithm is to resolve for k dominant reflectors, we first need to decide the ranges of θ_{mid} where these K dominant reflectors reside in. This is done by picking the K highest peaks in the curve $P_r^{\mathrm{m}}(\theta_{mid})$, as illustrated in Figure 4. Notably, the curve $P_r^{\mathrm{m}}(\theta_{mid})$ is obtained by using the fine-grained spatial scanning process. Specifically, the process steers the transmit antenna to point θ_{mid} to a sequence of N angles respectively, denoted by $\theta_1, \ldots, \theta_N$, which are evenly distributed between 0° and 360° with a step size $\omega = 360^\circ/N$, i.e., $\theta_i = i\omega$ for $1 \le i \le N$. At each θ_i, let the measured RSSI at the receiver be $P_r^{\mathrm{m}}(\theta_i)$. Recall that we are only interested in NLoS paths, so those θ_i's that belong to the LoS should be excluded in our subsequent range selection. Let the LoS direction be θ_{LoS}. Since the half beam width of the transmit antenna is Θ_{beam}, a θ_i is considered belonging to the LoS if $\theta_{LoS} - \Theta_{beam} \le \theta_i \le \theta_{LoS} + \Theta_{beam}$. For example, in Figure 4, the LoS direction θ_{LoS} is 330°, and the half beam width of antenna is 30°. So RSS measurements between 300° to 360° are considered belonging to the LoS range and are ignored during subsequent NLoS path ranges selection procedure.

Our range decision is iterative: we decide one non-overlapping range for θ_{mid} in each iteration, and our decision concludes after K iterations, resulting in K non-overlapping ranges. In particular, in the k-th iteration we decide a range $\left[\theta_{low}^{(k)}, \theta_{high}^{(k)}\right]$ that includes the following angles:

$$\theta_k^o = \arg\max \left\{ P_r^{\mathrm{m}}(\theta_i) \,\middle|\, \theta_i \notin \bigcup_{j=1}^{k-1} \left[\theta_{low}^{(j)}, \theta_{high}^{(j)}\right] \right\}. \quad (8)$$

And all adjacent θ_i's that are within the half beam of θ_k^o but are not included in any of the ranges decided in previous iterations, i.e., $\left[\theta_{low}^{(k)}, \theta_{high}^{(k)}\right]$ includes the following θ_i's:

$$\{\theta_i | \theta_k^o - \Theta_{beam} \le \theta_i \le \theta_k^o + \Theta_{beam}\} \text{ and } \theta_i \notin \bigcup_{j=1}^{k-1} \left[\theta_{low}^{(j)}, \theta_{high}^{(j)}\right], \quad (9)$$

where $\theta_{low}^{(k)}$ and $\theta_{high}^{(k)}$ are the smallest and the largest elements in the above set, respectively. A θ_i is excluded from the subsequent iterations if it has been included in one of the ranges decided in previous iterations. Note that by picking the above K ranges, we do not mean that the AoDs of the top-K dominant reflectors should reside in each of these K ranges (i.e., one in each range). Instead, the AoDs of the top-K dominant reflectors should reside in the union of these K ranges.

(2) High-resolution in-lobe resolving: Now that we have the top-K ranges of θ_{mid} as $\left[\theta_{low}^{(k)}, \theta_{high}^{(k)}\right]$, $1 \le k \le K$, we need to resolve the reflectors whose AoDs are within these ranges. Without loss of generality, let us consider the k-th range. Suppose there are N reflectors in this range, and accordingly there are N NLoS paths (this is because each reflector generates exactly one NLoS path via its specular reflection) in the cluster defined by this range. And each path can be characterized by its propagation (and reflection) path loss, AoD, and path phase shift, denoted by g_i, ϕ_i, and δ_i respectively, for the i-th NLoS path, where $1 \le i \le N$. Considering the beam width of the transmit antenna, notice that for the k-th range, we have $\theta_{low}^{(k)} - \Theta_{beam} \le \phi_i \le \theta_{high}^{(k)} + \Theta_{beam}$ for all $1 \le i \le N$. Given that the main beam of the transmit antenna is pointing at θ_{mid}, the transmit antenna gain for the i-th NLoS path is given by

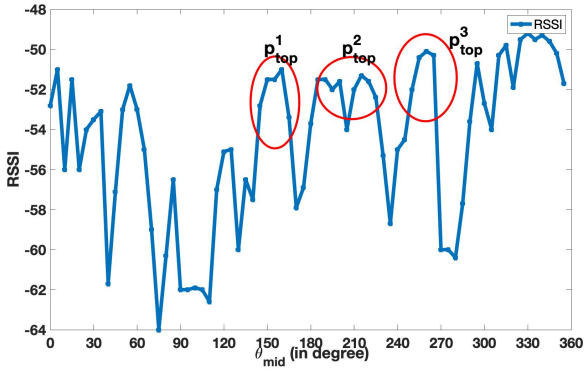

Fig. 4: Out-lobe resolving based on measured RSSI (scanning step $\omega = 5^\circ$).

$$D(\theta_{mid}|\phi_i) = \begin{cases} 1 & \phi_i - \Theta_{beam} \le \theta_{mid} \le \phi_i + \Theta_{beam} \\ 0 & \text{otherwise.} \end{cases} \quad (10)$$

Therefore, when the transmit antenna is scanning within the k-th range, the RSS at the receiver can be analytically described as

$$P_r(\theta_{mid}) = P_t \left\| \sum_{i=1}^{N} D(\theta_{mid}|\phi_i) g_i e^{j\delta_i} \right\|^2, \theta_{low}^{(k)} \le \theta_{mid} \le \theta_{high}^{(k)}. \quad (11)$$

To resolve for g_i's, ϕ_i's, and δ_i's, we use reverse engineering: we would like to decide the optimal g_i^o's, ϕ_i^o's, and δ_i^o's that would make $P_r(\theta_{mid})$ the closest match, in the mean square error (MSE) sense, with the measured RSS $P_r^{\mathrm{m}}(\theta_{mid})$ at the discrete angles $\theta_i \in \left[\theta_{low}^{(k)}, \theta_{high}^{(k)}\right]$, i.e.,

$$\underset{g_i^o, \phi_i^o, \delta_i^o, i \in N}{\text{minimize}} \sum_{\theta_i = \theta_{low}^{(k)}}^{\theta_{high}^{(k)}} \left| P_r(\theta_i) - P_r^{\mathrm{m}}(\theta_i) \right|^2. \quad (12)$$

In our evaluation part, the signal gain g is from -50 dB to -70 dB with step size 0.01 dB. The angle direction ϕ is from $[\theta_{low}^{(k)}, \theta_{high}^{(k)}]$ with a step size 0.1°. And phase δ is from 0° to 360° with a step size 0.1°

Compared with the global range (from 0 to 360°) reverse engineering in Eq.(7), the scale of the above local range optimization, in terms of the number of variables to be optimized, is much smaller therefore the optimization can be achieved much faster. This is for the ground truth number of reflectors in $\left[\theta_{low}^{(k)}, \theta_{high}^{(k)}\right]$ should be much smaller than that in $[0^\circ, 360^\circ]$, so a small N in Eq.(12) is usually sufficient to obtain small MSE in the objective function. To verify the point, we solve the optimization problem in Eq.(12) for the top-3 ranges highlighted in Figure 4 under various N's. As a representative outcome, Figure 5 plots the normalized MSE for the optimization in range 1 as a function of N, where the

normalization is w.r.t. the square of the maximum measured RSS in range 1. It can be observed that the normalized MSE in this case goes down quickly as N increases, and remains almost flat after $N \geq 3$, implying that $N = 3$ is an acceptable estimation for the ground truth number of major reflectors in this range. Note that our resolved top-N dominant reflectors are in fact dominant reflector clusters, each of which represents an aggregation of multiple closed-by reflectors and do not have one-to-one correspondence with actual physical reflectors. Both specular and diffusive (or scattering) reflection effects have already been aggregated into these reflector clusters.

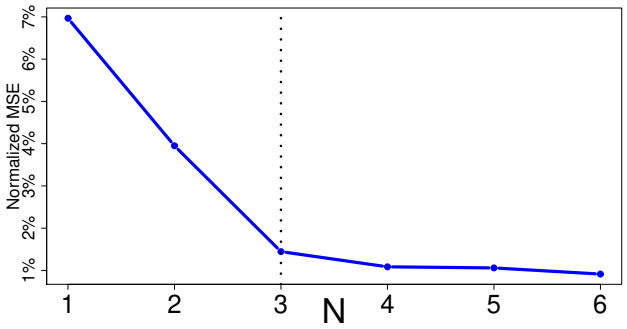

Fig. 5: Normalized MSE v.s. N.

The AoDs of the top-K dominant reflectors are decided by pooling the reflectors resolved over all K ranges together, and picking the top-K among them with the smallest propagation losses (i.e., highest g_i's). For example, Table 1 lists the optimized g_i's and ϕ_i's for the top-3 ranges in Figure 4 for $N = 3$. The optimized δ_i's are not shown in the table due to space limit. The top-3 dominant reflectors are decided as: Reflector 1 in range 1 (path loss = -55.83 dB, AoD = 172.5°), Reflector 1 in range 3 (path loss = -55.96 dB, AoD = 275.8°), and Reflector 3 in range 3 (path loss = -56.19 dB, AoD = 235.2°). Among them, it can be observed that the AoDs of the last two dominant reflectors are separated less than the beam width of the transmit antenna. These results verify that the proposed two-step algorithm can achieve fine-grained multi-path channel resolving by only using coarse-grained wide-beam antennas. We then use a real testbed to evaluate the accuracy of the resolved paths and their effects in maintaining mmWave connections in Section 3.

TABLE 1: Multi-path channel resolving result.

Par	g_1	ϕ_1	g_2	ϕ_2	g_3	ϕ_3
$P_{top}^{(1)}$	−55.83	172.5°	−57.60	134.4°	−60.37	152.3°
$P_{top}^{(2)}$	−61.47	210.9°	−56.84	196.8°	−56.54	243.2°
$P_{top}^{(3)}$	−55.96	275.8°	−58.15	257.8°	−56.19	235.2°

2.2.3 Localization for the client and the AP

Aiming for real-time beam switching under the mobile scenario, the accurate location information of the client and the AP is essential in the proposed framework. However, the GPS localization is not suitable for the indoor usage scenario. Moreover, the resolution of the GPS system is low, typically in several meters, which does not meet the precision requirement of our problem. To obtain high precision localization information, we use the HTC VIVE VR system to track the real-time location of the client. Note that the VR system can be replaced by any indoor mmWave device localization method, such as the mmWave AP triangulation [27] or AP device localization mentioned in [34].

2.2.4 Matching the AoDs

To fully determine a dominant reflector using our framework, we need at least three independent sets of $< \phi, (x_t, y_t) >$. Therefore, in an environment with multiple dominant reflectors, how to identify those AoDs that are measured at different client locations but are associated with the same dominant reflector raises another challenge.

To address this issue, we exploit the sparsity of the mmWave channel, which dictates that the mmWave channels at two nearby locations are caused by the same set of dominant reflectors. So their spatial channel profiles (SCPs) are tightly correlated in the sense that their AoD realizations associated with the same reflector are also close-by to each other [23]. To utilize this property, we propose the following AoD measurement and matching process. We fix the AP's location, and measure the RSSI at the AP as a function of θ_{mid} when the client is positioned at several nearby locations, respectively. Denote this set of nearby locations as set S. We then identify the top-K AoDs at the first client location based on the RSSI-θ_{mid} measurement made at that location. Let $\phi_1^{(1)}, \phi_2^{(1)}, \ldots, \phi_K^{(1)}$ denote these top-K AoDs, associated with K strong dominant reflectors, say $R_1, R_2, \ldots, R_K$, respectively. Let $\phi_i^{(j)}$ denote the AoD realization associated with reflector R_i at a different client location $j \in S$. To decide $\phi_i^{(j)}$, one simply finds the peak RSSI measured at client location j that is nearest to $\phi_i^{(1)}$. The θ_{mid} corresponding to this peak RSSI is $\phi_i^{(j)}$.

The above process is illustrated in Figure 6, where the RSSI-θ_{mid} measurements have been made at two close-by locations, represented by the blue curve and the red curve, respectively. To decide the AoD realizations of three strong dominant reflectors at these two locations, we first pick the top-3 AoDs on the blue curve, and label them as NLoS1 through NLoS3 in blue. Then, the AoD realization of NLoS1 on the red curve is simply the red peak nearest to the blue peak of NLoS1. The AoD realization of NLoS2 and NLoS3 on the red curve can be decided in a similar way.

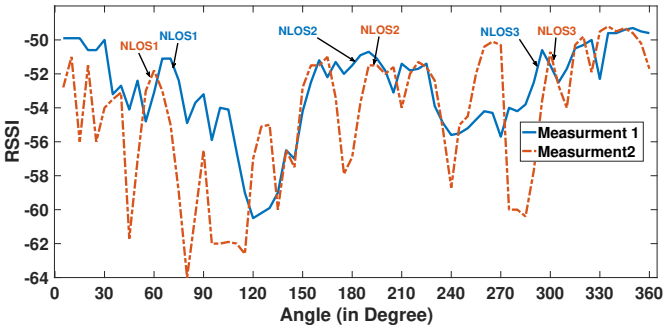

Fig. 6: NLoS path matching between two different client locations.

Based on our methods, we are able to obtain a sufficient number of $< \phi_i, (x_t, y_t) >$'s for each of the K strongest

dominant reflectors identified in the AoD matching process, based on which the proposed framework in Eq.(5) can be applied to calculate the location and orientation for each of these strong dominant reflectors.

2.3 Model Driven RSSI Estimation

In this section, we present a received signal strength estimation model to predict the link performance of the mmWave NLoS backup paths in real-time. When the LoS path is blocked, the aforementioned dominant reflector map provides K NLoS candidate paths for the transmit antenna to steer to. Selecting the best one among them will be critical to retain a comparable performance to that of the LoS path. However, the naive sequentially trial-based method will result in significant delays in beam switching, therefore undermining the stability of the connection. To achieve a better seamless beam switching performance, we use a model-driven approach on the transmitter side to predict the quality of each NLoS backup paths, so the transmit antenna can choose the best path directly.

Among the K NLoS candidate paths provided by the dominant reflector map, let us consider the one associated with the i-th dominant reflector. If the transmit antenna beam is switched to this path, then the received power P_r at the receiver is given by:

$$P_r = \frac{P_t G_t G_r}{L_f R_l}. \tag{13}$$

Here P_t is the total transmission power, G_t and G_r are the transmitter and receiver's antenna gain for the path; L_f and R_l are the free space loss and the reflection loss of the path, respectively. The total transmission power is a constant for a COTS device. The antenna gains are also fixed, because the receive antenna is omni-directional, and the path is in the main lobe of the transmit antenna (so $G_t = 1$). Next, we will explain how to calculate L_f and R_l.

1)Free space Loss: According to the Friis's law, the free space loss L_f is:

$$L_f(d) = \left(\frac{\lambda}{4\pi d}\right)^2, \tag{14}$$

where λ is the wavelength of the carrier frequency and d is the length of the NLoS path.

Our model considers the specular reflection, so the transmission path length d between the client and the AP is equal to the distance between the client and the virtual AP, which can be calculated using:

$$d = \sqrt{(x_t - x_r')^2 + (y_t - y_r')^2}, \tag{15}$$

where the virtual AP's location (x_r', y_r') is defined w.r.t. the i-th dominant reflector and is given by Eq.(2).

2)Reflection Loss: The reflection loss depends on the material of the reflector, and can be characterized using the Fresnel reflection coefficient(Γ) [35], [36]. There are two Fresnel equations for two different polarization cases. And we use a simplified version of the horizontally polarized model, under which the Fresnel coefficient is given by:

$$\Gamma_H = \frac{\sin\psi - \sqrt{\varepsilon_r - \cos^2\psi}}{\sin\psi + \sqrt{\varepsilon_r - \cos^2\psi}}, \tag{16}$$

where ε_r is the relative permittivity of the reflective material, ψ is the grazing angle. Notably, the ε_r remains as a constant and does not depend on the carrier frequency [35]. The grazing angle is the angle between the incident ray and the reflecting surface, since we have already modeled the reflector as a line segmentation $Ax+By+C=0$, the grazing angle can be calculated by:

$$\psi = \arctan\left(\left|\frac{k - \tan(\phi)}{1 + k\cdot\tan(\phi)}\right|\right), \tag{17}$$

where $k = -A/B$ is the slope of the reflector surface, ϕ is the specular ray AoD, given by:

$$\tan(\phi) = \frac{(B^2 - A^2)x_r - 2ABy_r - 2AC - (A^2 + B^2)x_t}{(A^2 - B^2)x_r - 2ABx_r - 2BC - (A^2 + B^2)y_t}, \tag{18}$$

where (x_t, y_t) is the real-time location of the client, and (x_r, y_r) is the location of the AP. The reflection loss can then be represented as [35]:

$$R_l = \left|\frac{1}{\Gamma_H}\right|^2 = \left|\frac{\sin\psi + \sqrt{\varepsilon_r - \cos^2\psi}}{\sin\psi - \sqrt{\varepsilon_r - \cos^2\psi}}\right|^2. \tag{19}$$

Note that the above theoretical model only describes the general pattern followed by the RSS on this path. To make this model fit in our particular operation environment, we use a regression for model parameter fitting. In particular, we consider the following decibel form of the RSS for the NLoS path associated with the i-th dominant reflector:

$$\begin{aligned} &P_r^{(i)}(d,\psi) = \\ &\kappa_i - 20\eta_i \log_{10}(d) - 20\gamma_i \log_{10}(\left|\frac{\sin\psi + \sqrt{\zeta_i - \cos^2\psi}}{\sin\psi - \sqrt{\zeta_i - \cos^2\psi}}\right|). \end{aligned} \tag{20}$$

We estimate the parameters κ_i, η_i, γ_i and ζ_i of the model offline using regression when the transmit beam is switched to the i-th dominant reflector with known AP and client locations (so d and ψ can be calculated). The data is gathered using the empirical RSSI readings generated by the device's firmware (unit in decibel). The regression functions $P_r^{(i)}(d,\psi)$, $i = 1,\ldots,K$, are then used online to model the received signal strength for the K NLoS paths offered by the dominant reflector map at new client locations. When the LoS is being blocked, our system can compute the RSS of different NLoS paths and directly switch the transmit beam to the best one among them.

2.4 Overhead/Cost Analysis

In this section, we provide a overhead/cost analysis for our proposed method. The total overhead of the system consists of the following two components:

1) Offline calibration phase: As we have discussed in Section 2.1, to fully determine the location and orientation of environmental reflectors, we need at least three independent sets of $< \phi, (x_t, y_t) >$ for algorithm processing. During the calibration phase, we fixed the AP location and move the client to three different locations to perform a 360° fine-grained spatial scanning. The scanning step is ω. For each step, we record the RSS from the AP side, so in total we collect $3 \cdot \frac{360^\circ}{\omega}$ RSS measurements. In our test, each RSS measurement is represented by a 4 byte float number, and ω is set to 5°, so the total information needed is 864 byte.

Low-resolution out-lobe resolving: In this part, for each $(360^\circ/\omega)$ number of RSS measurements, our algorithm determines K RSS ranges for high-resolution in-lobe resolving. An iterative approach is used to determine these K ranges, so the time complexity is $\mathcal{O}(K)$. Since the number of dominant reflectors in an indoor environment is usually limited, a small K is sufficient to provide stable NLoS paths for robust communication. In our experiments, we set K to 3 and the actual time spent by low-resolution out-lobe resolving process is negligible.

High-resolution in-lobe resolving: For each RSS range extracted from the low-resolution out-lobe resolving phase, it contains $(2\Theta_{beam}/\omega)$ RSS measurements, where Θ_{beam} denotes the half beam width of the main lobe. And we need to solve N sets of g_i^o's, ϕ_i^o's, and δ_i^o's for each selected range. In this step, we use an optimization tool to solve the proposed MMSE problem. In our test, we use the MatLab fmincon function with default interior-point method. We have validated that a small N (3 to 4) is usually sufficient to obtain a sufficient small error in the objective function. With an Apple iMac with 3.4 GHz Quad-Core Intel Core i5 CPU, the optimization can be done within 10 seconds for each range when N is set to 3.

RSSI Regression: For each of the K dominant reflectors, we estimate the parameters κ_i, η_i, γ_i and $\zeta_i, i \in K$ of the model offline using regression when the transmit beam is switched to the i-th dominant reflector with known AP and client locations. The data is gathered using the empirical RSSI readings generated by the device's firmware. In our evaluation part, 10 to 15 different client locations are enough for the regression model to reach a high accuracy. The regression is performed by using the MatLab curving fitting with the nonlinear least-squares fitting procedure. With an Apple iMac with 3.4 GHz Quad-Core Intel Core i5 CPU, the regression can be done within 1 seconds for each range when K is set to 3.

2) Online operation phase: In the online operation phase, our algorithm uses specular reflection model to calculate the NLoS paths for current locations. The time complexity to calculate K paths is $\mathcal{O}(K)$.

The complexity analyses are summarized in table 2

Phase	Operation	Complexity
Offline sensing	Fine-grained 360° scanning	$\mathcal{O}(\frac{360^\circ}{\omega})$ for 3 times
	Low-resolution out-lobe resolving	$\mathcal{O}(K)$ for each scanning
	High-resolution in-lobe resolving	Fmincon with interior-point method
	Path loss regression	Nonlinear least-squares fitting
Online operation	NLoS paths calculation and switching	$\mathcal{O}(K)$ to calculate K paths

TABLE 2: Complexity of each step.

2.5 Limitation of the Method and Extension to Larger space

A dominant reflector is defined naturally in a local sense, because the strength of its reflected signal will go down with the distance between the reflector and the user increases. So a reflector being dominant when the user was close may not remain dominant when the user moves far away. Because of this, our proposed method can only be directly applied to a small-to-moderate room scenario, where at least one reflector defined in the top-K dominant reflector map remains to be dominant at any location of the room. In reality, this may correspond to practical application scenarios such as wireless VR/AR gaming, in which a player does not move too far but may frequently turn their body, or multiple players interact with each other in one game, so the LoS may be frequently blocked by the player's or the other player's body. In the multi-user scenario, other users can not only block the LoS but also the estimated NLoS path with each other. This issue can be trivially solved by simply turning to the second or next optimal estimated NLoS direction, as the proposed method is actually able to compute the top-K optimal NLoS directions based on the top-K dominant reflector map.

The proposed method can be trivially extended to a larger-space scenario (e.g., a ballroom or an auditorium) by partitioning the space of the room into smaller areas, and then applying the proposed method to each area to construct a individual dominant reflector map. The maps of individual areas are then aggregated and fused into a master map that describes the location and reflection efficiency of all dominant reflectors in the room. This master map is distributed to each user in the operational phase for their online strong NLoS path prediction and beam switching. Such an extension is out of the scope of this work and will be pursued in our future research.

Also, we want to point out that our proposed mechanism is suitable for most of the indoor household application scenarios, where the room layout (i.e., the environment) is static or quasi-static but the users could be moving. For instance, when a user is playing an electronic VR game or using wireless cell phone in indoor environment, the direction of the strongest NLoS path keeps changing due to the user's movement but the environment is static (i.e., the locations of the dominant reflectors do not change or remain static for a long period of time). This static environment assumption should be true in most of the indoor application scenarios, because those major reflectors are usually large-size furniture, walls, and windows of metallic surfaces, which are hardly mobile.

3 Testbed and Implementation

We implemented our prototype system based on COTS components. The system architecture and prototype are shown in Figure 7. Our system consists of four main parts: 1) two MikroTik WAP 60G mmWave radios [28] are used for mmWave communication; 2) a robotic arm is used for 360° mechanical steering of the transmit beam. This robotic arm is needed only during the one-time offline site survey (installation) phase to perform stepped scanning. In the online operational phase, this robotic arm is optional. If it is not available, the COTS device can simply steers the transmit beam to the particular beam mode (e.g., 64 beam modes are provided by MikroTik WAP 60G) that is the closest to and covers the desired NLoS direction, achieving an approximation to the original mechanism presented in Section 2 when the arm is available to steer the beam to the

exact desired direction. 3) A VR system is used to provide accurate position information for the AP and the client. Note that this VR system is used only for convenience/ease of our implementation. It can be replaced by any state-of-the-art indoor WiFi-based localization algorithm that does not require any additional infrastructure [27]; 4) a PC host is used to control the beam switching procedure according to our proposed method.

Our testbed is only intended to serve as a prototype to demonstrate the feasibility of the proposed method. The robotic arm is not an indispensable part to perform our algorithm. In particular, in the online NLoS prediction phase, instead of using the robotic arm for fine-grained mechanical steering of the antenna beam, the COTS firmware we are using allows a coarse-grained electronic steering of the beam by selecting an appropriate beam pattern that covers the desired direction to which the beam should be turned. In the offline measurement phase, using the robotic arm to do the automatic space scanning can significantly expedite the measurement process. However, in case that the robotic arm is not available, the above scanning can also be done manually.

When the LoS is blocked, in order to allow the user to turn its beam to the estimated NLoS direction, say α, we do need to know the direction/orientation of the beam right before the LoS blockage, i.e., the direction of the LoS path, denoted as β. So after the blockage the beam needs to turn $\alpha - \beta$ degrees from its current orientation in order to point to the estimated NLoS direction. Given the availability of the locations of the AP (denoted as (x_0, y_0)) and the user(denoted as (x_1, y_1)), the orientation of the user's beam before the LoS blockage can be calculated as $\beta = \arctan \frac{x_1 - x_0}{y_1 - y_0}$ (without loss of generality, here we are assuming that the direction of the Y-axis is the $0°$).

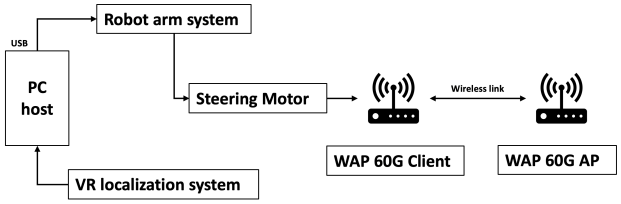

(a) Testbed architecture.

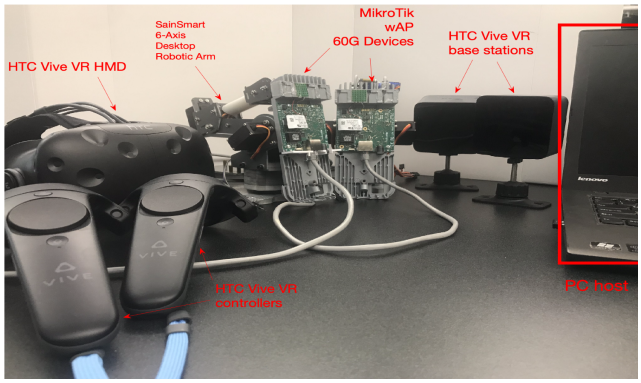

(b) Testbed overview.

Fig. 7: System prototype.

4 Evaluation

4.1 Test Setting

Test environment: The performance test is conducted in an indoor lab with a 4.9 m $\times$ 4.8 m layout. We set up a pair of AP and client. The AP is placed at a fixed location with coordinate $(-1.44, 0.05)$, and its receive antenna is omni-directional. For the client, its location is random picked to cover the whole test area and a VR HMD is bounded with the client to track its location(VR base stations are mounted on wall for HMD position tracking). The client uses a beam-forming mode that forms a $60°$ beam for transmission. We use the iPerf as the traffic source to drive the mmWave link, and the RSSI measurement is extracted from the integrated RouterOS operating system.

Reflectors reconstruction: To reconstruct dominant reflectors, we need multiple correlated tests to fully locate them. So we fix the AP to an anchor location and move the client to three different locations to perform a $360°$ scanning with a step angle $5°$. The measured RSSI patterns are fed as input for the two-step AoD derivation method to extract the AoDs of dominant reflectors. Then we use these AoDs and location information as the input for specular reflection model to reconstruct the dominant reflectors' geometry.

The NLoS path directions are calculated using dominant reflectors' geometry and real-time client locations. To compare the performance of different NLoS paths, we conduct a link performance test under 30 different client locations and use the RSSI as the performance metric. In addition, a transport layer performance test under TCP/UDP, containing both static and mobile scenarios, is also conducted to show the performance of our system under different conditions. In the static test, both the AP and client's locations are fixed, whereas in mobile scenario, only the AP's location is fixed and the client moves across the room with 0.5 m/s velocity. The real time TCP/UDP throughput is used as the performance metric.

Performance benchmarks: For the purpose of performance comparison, we conduct two types of performance benchmarks. The first is the performance using LoS link for communication, which is the upper bound performance of the system. The second is the performance using auto beam steering method [37], which is the default beam steering method for the MikroTik WAP 60G devices. The method follows the IEEE 802.11ad standard and can automatically change the beam among the 64 predefined beam patterns to maximize the throughput.

4.2 Experimental Results

4.2.1 *Dominant Reflector Reconstruction*

In our test, we successfully reconstruct two dominant reflectors, namely the left side reflector 1 and bottom side reflector 2, as specified in Figure 8. The reflection coefficients obtained by our regression model is 1 and 0.224 for reflector 1 and reflector 2. The rectangle denotes the lab's layout. The blue and red lines represent the two reconstructed dominant reflectors.

4.2.2 *Link Performance Test*

After locating the dominant reflectors in the environment, we set the AP to the anchor position as in Figure 8 and

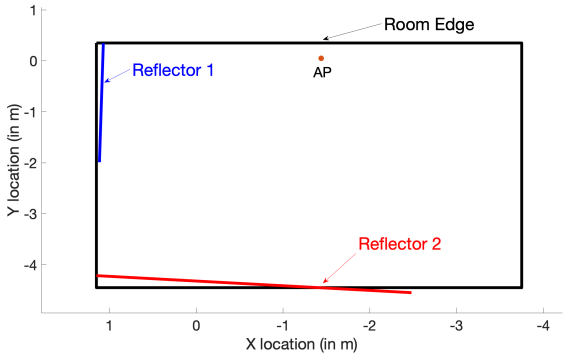

Fig. 8: Dominant reflector map.

randomly select client test locations to conduct a comprehensive performance test. For each test location, we first measure the RSSI value of the LoS link under the blockage, then we calculate two NLoS directions corresponding to those two reflectors. A high RSSI value usually indicates a better channel status. For a LoS link without any blockage, the average RSSI value is -50 dB. Figure 9 plots the RSSI color maps for four different beam steering strategies under LoS blockage.

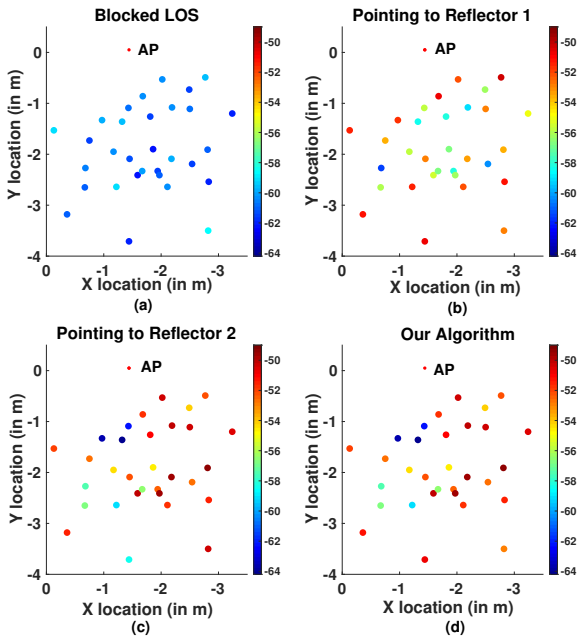

Fig. 9: RSSI color map.

Figure 9a shows the performance under no beam steering strategy. We refer this as the baseline performance. The average RSSI drop is -12 dB. At some test points, the link even suffers from outage. Intuitively, we would think a broad width beam pattern to be beneficial to stabilize the linkage. However, in our test, a broad width beam pattern does not mitigate the performance drop when blockage happens. The finding indicates the LoS link is no longer available for stable mmWave communication under the blockage.

Figure 9b shows the performance when the beam direction changes to reflector 1's specular reflection direction. These paths are denoted as $NLoS_1$. In this case, the RSSI values are acceptable for most of the test locations. We observe that test points at the center of the environment usually have lower RSSI values comparing to other points. A possible reason is that although reflector 1 can always create available NLoS links, the performance for different NLoS links highly depend on the client locations.

Figure 9c shows the performance when the beam direction changes to reflector 2's specular reflection direction. These paths are denoted as $NLoS_2$. Compared to Figure 9b, the performance is better for most of the test locations. As mentioned before, the performance of the NLoS link highly depends on the reflector's physical properties, such as the material and area size. Reflector 2 contains a metal cabinet, which has a larger reflective area than that of reflector 1.

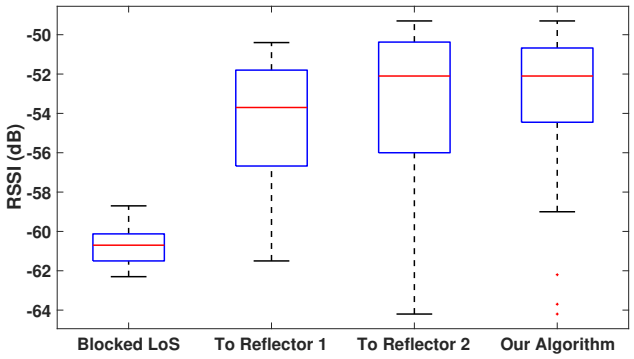

Fig. 10: Performance of different NLoS links.

Figure 9d shows the result of our proposed beam steering algorithm, where the NLoS link is selected based on estimated RSSI values of different NLoS paths. The overall performance is better than using either $NLoS_1$ or $NLoS_2$.

Figure 10 shows the numerical results of Figure 9. The average RSSI of the LoS blockage case is -61 dB, which is far below that of $NLoS_1$ or $NLoS_2$. $NLoS_2$ has a higher average RSSI value compared to that of $NLoS_1$(-52.1 dB over -53.5 dB). The RSSI values of $NLoS_1$ are bounded by a tighter range, indicating a greater stability. Our algorithm takes advantage of both reflectors. The average RSSI measured using our system is -52.1 dB, which is the same as the $NLoS_2$. The distribution of the RSSI values is less dispersed. In addition, most of the measurement locations achieve RSSI strength higher than -55 dB, which is a huge performance boost compared to the baseline.

Figure 11 shows the CDF of RSSI. From left to right, the lines represent the RSSI of ground truth, our system and LoS link under blockage, respectively. The ground truth is generated by comparing the NLoS link measurement result in each test location and choose the highest RSSI value, which is treated as the oracle value of the current location. The performance of our system is close to the oracle value, which indicates our system can successfully choose the best NLoS link by predicting the link performance using the RSSI estimation model.

4.2.3 *Evaluation of Path RSSI Estimation Model*

The RSSI estimation model is an essential part in deciding the best NLoS path direction, so we compare our prediction results with the real world measurements. Figure 12

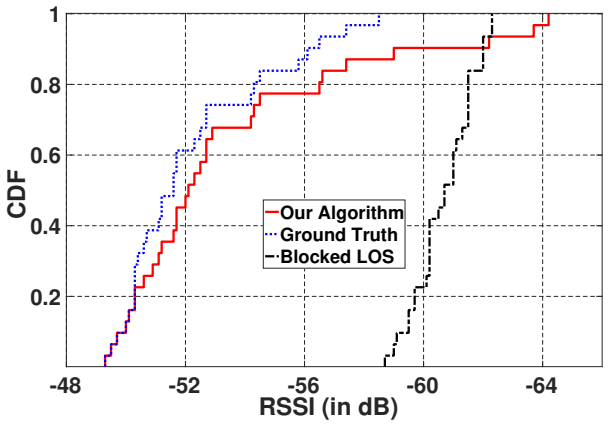

Fig. 11: RSSI distribution.

illustrates the RSSI estimation model accuracy for the two dominant reflectors. The horizontal axis refers to the estimation error. For both reflectors, about 80% RSSI estimation errors are below 4 dB, and 40% are below 2 dB. Therefore, our RSSI estimation model accurately estimates the RSSI measurement, and thus efficiently assists our system in selecting the best NLoS.

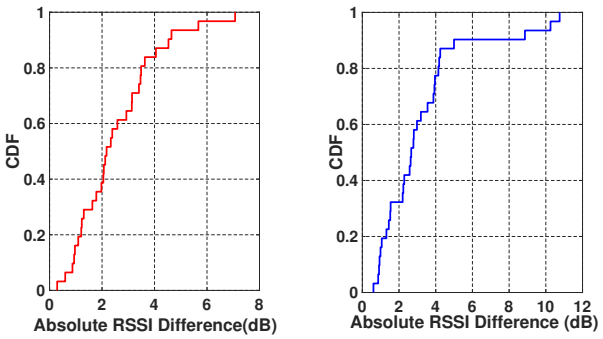

(a) Reflector 1 (b) Reflector 2

Fig. 12: The CDF of RSSI estimation error.

4.2.4 *System Performance under Static and Mobile Scenarios*

Our system is designed to handle indoor mobile device communication, such as VR gaming. So we use a bandwidth testing software (integrated in the WAP 60G system) to conduct a transport layer throughput test. To provide more convincing results, we test our system on both UDP and TCP. For all test scenarios, the LoS link test is conducted without any blockage to serve as the upper bound performance, and the LoS direction is blocked by human bodies to test the performance under blockage.

Static scenario performance test: We first perform a static test where we fix the locations of client and AP. The purpose is to test the performance for different methods under a static scenario where the LoS is blocked and each method tries to recover the high performance.

Figure 13 shows the bandwidth test results of four methods. The "LoS", "Ours", "Blocked LoS" and "Auto" represent the throughput measured by the LoS link, our system, LoS being blocked and auto beam steering method, respectively. For each method, we conduct a 60-second

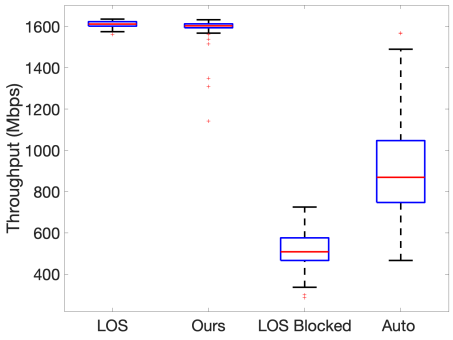

(a) UDP test.

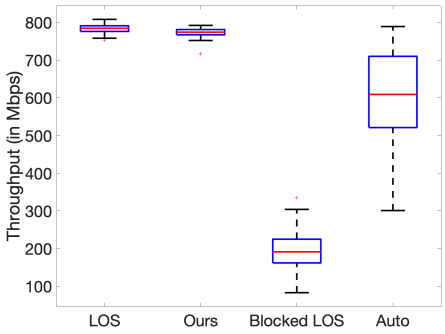

(b) TCP test.

Fig. 13: Transport layer throughput trace in UDP.

bandwidth test and record the throughput sequence. The UDP result is shown in Figure 13a, the average throughput of "LoS" is 1612 Mbps, and the throughput is stable, as the LoS link is the most reliable link. The average throughput of "Ours" is very close to that of "LoS", which is 1603 Mbps. The "Blocked LoS" shows that as the RSSI values suffer from a drastic degradation when blockage, the throughput also drops dramatically. The average throughput is only 503 Mbps, which is about only 30% of the throughput of "Ours". The "Auto" method, which automatically select a beam pattern among the 64 pre-defined patterns to maximize the throughput, has a higher average throughput (869 Mbps) than that of "Blocked LoS", but only 50% of "Ours". The distribution of the "Auto" spread widely, with a minimum value 466 Mbps and maximum value of 1569 Mbps.

Figure 13b shows the TCP test results. Compared to UDP, TCP is more reliable and can tolerate severer signal strength drop. In compensation, the maximum TCP throughput is lower than that of UDP. This is reflected in our result that the average throughput for the "LoS" in TCP (791 Mbps) is about half value of that in UDP. Similar to UDP case, the average throughput of "Ours" in TCP (774 Mbps) is very close to the "LoS" in TCP (791 Mbps). Compared to UDP, the throughput of "Auto" in TCP is closer to "LoS".

The "Ours" method has a higher TCP/UDP throughput than the "Auto" method since "Ours" can achieve higher RSSI values than the "Auto" method. To justify this point, we test the RSSI of "Ours" and "Auto" under a static scenario and plot the measured RSSIs in Figure 14. More specifically, our test is performed under a static scenario where we block the LoS at 15 random locations and collect

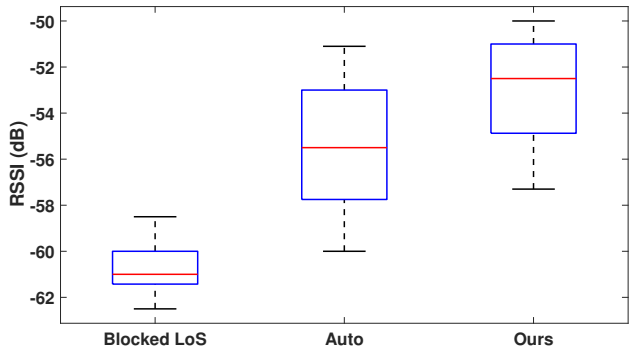

Fig. 14: Performance comparison with RSSI.

the RSSIs under "Ours" and "Auto" methods respectively at each location. The RSSI of the blocked LoS is also collected to provide a baseline for the comparison. When the LoS is blocked, the average RSSI of the LoS link drops to -60.6 dB. While both the "Auto" and "Ours" methods bring in some RSSI gains over the blocked LoS, the "Ours" method can achieve a higher RSSI than the "Auto" method. In particular, as shown in Figure 14, the average RSSI of "Auto" is -55.4 dB, while the average RSSI of "Ours" is -52.8 dB, so a 2.6 dB gain over the "Auto" method. In addition, it can be observed that the variance of RSSI under "Ours" is smaller than that of the "Auto", which indicates that the performance of "Our" is more consistent at different locations than that of the "Auto" method.

The throughput result of "Ours" should be considered as the upper bound performance of our proposed method, which can be achieved when fine-grained steering of the beam (either electronically or mechanically) is available. Note that such an upper bound cannot be achieved by the "Auto" search method, even if fine grained beam steering is available (e.g., by having more higher-resolution patterns in the codebook). This is because a finer grained beam scanning will require the "Auto" method to scan through a larger number of beam patterns, and thus increases the delay for the method to select the optimal pattern, undermining the overall average throughput (where the increased delay should be accounted for as overhead) that can be achieved by the method. On the other hand, when fine grained beam steering is not available to our proposed method, our method will directly pick the pattern in the codebook that covers the estimated optimal NLoS direction. In this case, our method still outperforms the "Auto" method due to its much shorter beam switching delay and faster response time.

In summary, our system outperforms other methods from stability and throughput perspectives, in UDP, TCP and RSSI.

Mobile scenario performance test: We conduct a system level usage test, using TCP and UDP throughput as evaluation metrics. We fix the AP position and move the client across the lab. We conduct a 90-second system test: no blockage to the LoS direction in the first 30 s (0-30 s); human body blockage to the LoS direction continuously following the client movement in the second 30 s (30 s-60 s); blockage moved away from LoS direction in the third 30 s (60 s-90 s).

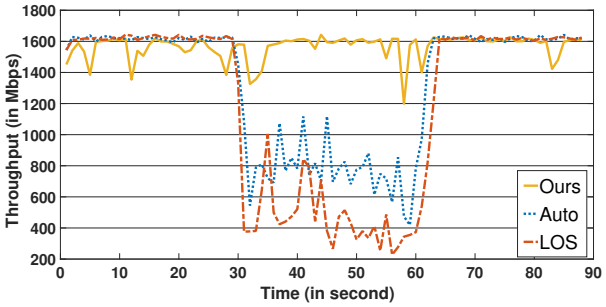

(a) UDP 90 s test.

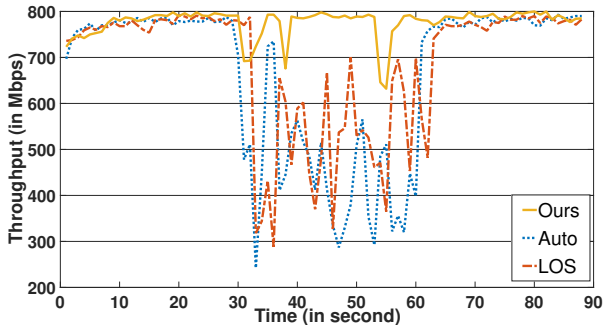

(b) TCP 90 s test.

Fig. 15: Transport layer throughput trace in TCP.

We also test the auto beam steering method for performance comparison.

Figure 15a shows the test result based on UDP. During the first 30 s, due to no blockage, all three methods select the LoS link for communication. Hence all methods reach a throughput of 1600 Mbps. Then the LoS link is blocked during the second 30 s. When a blockage happens, both "Auto" and "LoS" suffer from instantaneous performance drop. Due to the fact that the "LoS" only uses the direct LoS direction whereas the "Auto" selects among different beam patterns to maximize the throughput, the performance for "Auto" is better than "LoS" when blockage happens. However, both "Auto" and "LoS" throughput drop below 800 Mbps, which is only 50% of the maximum speed of the system.

As for our system, the throughput slightly drops when the blockage occurs. Then the throughput swiftly restores close to the maximum throughput, which is around 1600 Mbps. The overall throughput is stable during entire blockage period, but there still exist some unstable points. This is because the NLoS path signal strength is not uniformly distributed in the environment. Therefore, the throughput fluctuates as the client goes through strong and weak NLoS signal strength areas. This is consistent with our previous finding in Figure 9: the NLoS link performance highly depends on the client's location. In the meantime, the client changes the beam direction accordingly to maintain the high performance. We remove the blockage at the 60th second, bringing the LoS link available again. So all three methods can use the LoS direction and the throughput restores to the maximum level.

Figure 15b shows the TCP test results under the same test setting. Due to the error handling mechanism in TCP, the performance drop of "Auto" and "LoS" during the 30 s to 60 s is less compared to that of UDP, but still catastrophic

for the mmWave communication.

Similar to UDP case, our system can maintain a throughput to an "almost LoS link" (800 Mbps) throughput level with a little fluctuation. Our system shows a superiority in stability and performance aspects.

In summary, our system successfully handles the LoS blockage under mobile scenarios for COTS mmWave devices and provides robust link for mmWave communication.

5 Conclusions

In this paper, we develop a NLoS beam switching algorithm for off-the-shelf mmWave devices to maintain a stable connection when its LoS communication path is blocked. The main idea of our method is to leverage the sparsity of the mmWave channel and the spatial correlation of the close-by mmWave channels to resolve for the location and orientation of the dominant reflectors in the environment. Strong NLoS backup paths are then computed based on these resolved dominant reflectors. We also propose a model-driven RSSI estimation algorithm, which allows the transmitter to predict the quality of each backup NLoS path and pick the best one among them.

In contrast to existing methods, our model does not rely on high precision phased array antennas, nor does our model require accurate phase information of the received signals, and therefore is applicable to a wide line of COTS mmWave products. We validate the feasibility and effectiveness of our system on a mmWave off-the-shelf testbed and demonstrate that it supports efficient and stable mmWave communication under human blockage.

Our system can serve as a prototype for off-the-shelf mmWave devices to handle the LoS blockage. The simplicity and low cost of our system can benefit a wide range of low-end commercial mmWave devices.

Acknowledgments

This work is supported in part by NSF under grants CNS-2006998, CNS-1837034, and CNS-1745254. Any opinions, findings, conclusions, or recommendations expressed in this paper are those of the author(s) and do not necessarily reflect the views of NSF.

References

[1] A. Gupta and R. K. Jha, "A survey of 5g network: Architecture and emerging technologies," *IEEE access*, vol. 3, pp. 1206–1232, 2015.

[2] T. S. Rappaport, S. Sun, R. Mayzus, H. Zhao, Y. Azar, K. Wang, G. N. Wong, J. K. Schulz, M. Samimi, and F. Gutierrez, "Millimeter wave mobile communications for 5g cellular: It will work!" *IEEE access*, vol. 1, pp. 335–349, 2013.

[3] T. S. Rappaport, "5g millimeter wave wireless: Trials, testimonies, and target rollouts," in *IEEE Infocom*, 2018.

[4] A. Y. Ding and M. Janssen, "5g applications: Requirements, challenges, and outlook," *arXiv preprint arXiv:1810.06057*, 2018.

[5] Y. Niu, Y. Li, D. Jin, L. Su, and A. V. Vasilakos, "A survey of millimeter wave communications (mmwave) for 5g: opportunities and challenges," *Wireless networks*, vol. 21, no. 8, pp. 2657–2676, 2015.

[6] T. S. Rappaport, Y. Xing, G. R. MacCartney, A. F. Molisch, E. Mellios, and J. Zhang, "Overview of millimeter wave communications for fifth-generation (5g) wireless networks—with a focus on propagation models," *IEEE Transactions on Antennas and Propagation*, vol. 65, no. 12, pp. 6213–6230, 2017.

[7] R. Ford, M. Zhang, M. Mezzavilla, S. Dutta, S. Rangan, and M. Zorzi, "Achieving ultra-low latency in 5g millimeter wave cellular networks," *IEEE Communications Magazine*, vol. 55, no. 3, pp. 196–203, 2017.

[8] E. Bastug, M. Bennis, M. Médard, and M. Debbah, "Toward interconnected virtual reality: Opportunities, challenges, and enablers," *IEEE Communications Magazine*, vol. 55, no. 6, pp. 110–117, 2017.

[9] A. Prasad, M. A. Uusitalo, D. Navrátil, and M. Säily, "Challenges for enabling virtual reality broadcast using 5g small cell network," in *2018 IEEE Wireless Communications and Networking Conference Workshops (WCNCW)*. IEEE, 2018, pp. 220–225.

[10] G. R. MacCartney and T. S. Rappaport, "73 ghz millimeter wave propagation measurements for outdoor urban mobile and backhaul communications in new york city," in *2014 IEEE international conference on communications (ICC)*. IEEE, 2014, pp. 4862–4867.

[11] G. R. MacCartney, S. Deng, and T. S. Rappaport, "Indoor office plan environment and layout-based mmwave path loss models for 28 ghz and 73 ghz," in *2016 IEEE 83rd vehicular technology conference (VTC Spring)*. IEEE, 2016, pp. 1–6.

[12] S. Singh, F. Ziliotto, U. Madhow, E. Belding, and M. Rodwell, "Blockage and directivity in 60 ghz wireless personal area networks: From cross-layer model to multihop mac design," *IEEE Journal on Selected Areas in Communications*, vol. 27, no. 8, pp. 1400–1413, 2009.

[13] S. Kutty and D. Sen, "Beamforming for millimeter wave communications: An inclusive survey," *IEEE Communications Surveys & Tutorials*, vol. 18, no. 2, pp. 949–973, 2015.

[14] K. Ramachandran, N. Prasad, K. Hosoya, K. Maruhashi, and S. Rangarajan, "Adaptive beamforming for 60 ghz radios: Challenges and preliminary solutions," in *Proceedings of the 2010 ACM international workshop on mmWave communications: from circuits to networks*, 2010, pp. 33–38.

[15] S. Rajagopal, S. Abu-Surra, and M. Malmirchegini, "Channel feasibility for outdoor non-line-of-sight mmwave mobile communication," in *2012 IEEE vehicular technology conference (VTC Fall)*. IEEE, 2012, pp. 1–6.

[16] J. Palacios, D. De Donno, and J. Widmer, "Tracking mm-wave channel dynamics: Fast beam training strategies under mobility," in *IEEE INFOCOM 2017-IEEE Conference on Computer Communications*. IEEE, 2017, pp. 1–9.

[17] Y. M. Tsang, A. S. Poon, and S. Addepalli, "Coding the beams: Improving beamforming training in mmwave communication system," in *2011 IEEE Global Telecommunications Conference-GLOBECOM 2011*. IEEE, 2011, pp. 1–6.

[18] W. Yuan, S. M. Armour, and A. Doufexi, "An efficient and low-complexity beam training technique for mmwave communication," in *2015 IEEE 26th Annual International Symposium on Personal, Indoor, and Mobile Radio Communications (PIMRC)*. IEEE, 2015, pp. 303–308.

[19] Y. Huo, X. Dong, W. Xu, and M. Yuen, "Enabling multi-functional 5g and beyond user equipment: A survey and tutorial," *IEEE Access*, vol. 7, pp. 116 975–117 008, 2019.

[20] W. Wu, Q. Shen, M. Wang, and X. Shen, "Performance analysis of ieee 802.11. ad downlink hybrid beamforming," in *2017 IEEE International Conference on Communications (ICC)*. IEEE, 2017, pp. 1–6.

[21] B. Coll-Perales, M. Gruteser, and J. Gozalvez, "Evaluation of ieee 802.11 ad for mmwave v2v communications," in *2018 IEEE Wireless Communications and Networking Conference Workshops (WCNCW)*. IEEE, 2018, pp. 290–295.

[22] S. Sur, X. Zhang, P. Ramanathan, and R. Chandra, "Beamspy: Enabling robust 60 ghz links under blockage," in *13th USENIX Symposium on Networked Systems Design and Implementation (NSDI 16)*. Santa Clara, CA: USENIX Association, Mar. 2016, pp. 193–206. [Online]. Available: https://www.usenix.org/conference/nsdi16/technical-sessions/presentation/sur

[23] A. Zhou, X. Zhang, and H. Ma, "Beam-forecast: Facilitating mobile 60 ghz networks via model-driven beam steering," in *IEEE INFOCOM 2017-IEEE Conference on Computer Communications*. IEEE, 2017, pp. 1–9.

[24] R. Schmidt, "Multiple emitter location and signal parameter estimation," *IEEE transactions on antennas and propagation*, vol. 34, no. 3, pp. 276–280, 1986.

[25] R. Roy and T. Kailath, "Esprit-estimation of signal parameters via rotational invariance techniques," *IEEE Transactions on acoustics, speech, and signal processing*, vol. 37, no. 7, pp. 984–995, 1989.

[26] T. Wei, A. Zhou, and X. Zhang, "Facilitating robust 60 ghz network deployment by sensing ambient reflectors," in *14th {USENIX} Symposium on Networked Systems Design and Implementation ({NSDI} 17)*, 2017, pp. 213–226.
[27] G. Bielsa, J. Palacios, A. Loch, D. Steinmetzer, P. Casari, and J. Widmer, "Indoor localization using commercial off-the-shelf 60 ghz access points," in *IEEE INFOCOM 2018-IEEE Conference on Computer Communications*. IEEE, 2018, pp. 2384–2392.
[28] (2019, mar) wap 60g ap. [Online]. Available: https://mikrotik.com/product/wap_60g_ap
[29] M. E. Rasekh, Z. Marzi, Y. Zhu, U. Madhow, and H. Zheng, "Noncoherent mmwave path tracking," in *Proceedings of the 18th International Workshop on Mobile Computing Systems and Applications*, 2017, pp. 13–18.
[30] D. Steinmetzer, D. Wegemer, M. Schulz, J. Widmer, and M. Hollick, "Compressive millimeter-wave sector selection in off-the-shelf ieee 802.11 ad devices," in *Proceedings of the 13th International Conference on emerging Networking EXperiments and Technologies*, 2017, pp. 414–425.
[31] M. E. Rasekh and U. Madhow, "Noncoherent compressive channel estimation for mm-wave massive mimo," in *2018 52nd Asilomar Conference on Signals, Systems, and Computers*. IEEE, 2018, pp. 889–894.
[32] W. U. Bajwa, J. Haupt, A. M. Sayeed, and R. Nowak, "Compressed channel sensing: A new approach to estimating sparse multipath channels," *Proceedings of the IEEE*, vol. 98, no. 6, pp. 1058–1076, 2010.
[33] J. Choi, "Beam selection in mm-wave multiuser mimo systems using compressive sensing," *IEEE Transactions on Communications*, vol. 63, no. 8, pp. 2936–2947, 2015.
[34] K. Bigdely-Shamloo, "How to get raw (positional) data from htc vive?" Aug 2017. [Online]. Available: https://www.codeproject.com/Articles/1171122/How-to-Get-Raw-Positional-Data-from-HTC-Vive
[35] Y. Yaman and P. Spasojevic, "An intra-cluster model with diffuse scattering for mmwave communications: Rt-icm," *arXiv preprint arXiv:1905.08295*, 2019.
[36] S. J. Orfanidis, "Electromagnetic waves and antennas," 2002.
[37] "Manual:interface/w60g," 2018. [Online]. Available: https://wiki.mikrotik.com/wiki/Manual:Interface/W60G

Xueyang Hu Xueyang Hu received his B.S degree in Information Engineering from Xi'an Jiaotong University, China in 2017. He received M.S degree in Computer Science and Software Engineering from Auburn University, USA in 2020. He is currently pursuing the Ph.D. degree in the Department of Computer Science and Software Engineering at Auburn University. His research interests mainly focus on 5G mmWave communication and optimization in wireless network.

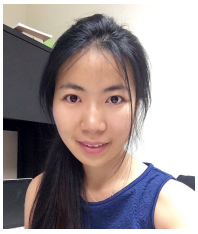

Tian Liu Tian Liu received her B.S. degree in Mathematics and Applied Mathematics from Sichuan University, China in 2011. She is currently pursuing the Ph.D. degree in the Department of Computer Science and Software Engineering at Auburn University. Her research interests focus on security and privacy issues in machine learning algorithms on IoT and CPS.

Tao Shu Tao Shu is currently an associate professor in the Department of Computer Science and Software Engineering at Auburn University. He received his Ph.D. in Electrical and Computer Engineering from The University of Arizona in 2010. He received the B.S. and M.S. degrees in Electronic Engineering from the South China University of Technology, Guangzhou, China in 1996 and 1999, respectively, and the Ph.D. degree in Communication and Information Systems from Tsinghua University, Beijing, China in 2003. Prior to his academic position, he was a senior engineer in Qualcomm Atheros Inc. from Dec. 2010 to Aug. 2011. His research aims at addressing security and performance issues in wireless networking systems, with strong emphasis on system architecture, protocol design, and performance modeling and optimization.